Adaptive Sliding Mode for Agile Attitude Tracking in a High-Precision Modelled VLEO Environment

Materials Research Proceedings 69 (2026) 1083-1088 https://doi.org/10.21741/9781644904251-187

Adaptive Sliding Mode for Agile Attitude Tracking in a High-Precision Modelled VLEO Environment

Pierantonio BERTUCCIO[1,a †*], Vincenzo Maria CANNAVALE[2,b †], Mattia ILLIANO[2,c †], Tobia Armando LA MARCA[3,d], Mauro MANCINI[1,e], Maria Daniela GRAZIANO[2,f], Elisa CAPELLO[1,g], Michele GRASSI[2,h]

[1]Department of Mechanical and Aerospace Engineering, Politecnico di Torino, Corso Duca degli Abruzzi 24, Torino, 10129, Italy

[2]Department of Industrial Engineering, University of Naples “Federico II”, Piazzale Tecchio 80, 80125, Napoli, Italy

[3]Scuola Superiore Meridionale, University of Naples “Federico II”, Largo San Marcellino 10, 80138, Napoli, Italy

[a]pierantonio.bertuccio@polito.it, [b]vincenzomaria.cannavale@unina.it, [c]mat.illiano@studenti.unina.it, [d]tobiaarmando.lamarca-ssm@unina.it, [e]mauro.mancini@polito.it, [f]mariadaniela.graziano@unina.it, [g]elisa.capello@polito.it, [h]michele.grassi@unina.it

† These authors contributed equally to this work

Keywords: VLEO, Spacecraft Attitude Control, Sliding Mode Control, Adaptive Control

Abstract. This paper presents a novel Sliding Mode Control (SMC) control formulated on the special orthogonal group SO(3) for spacecraft attitude control in Very Low Earth Orbit (VLEO). The approach addresses nonlinear rotation geometry and environmental disturbances without the singularities or redundancy of traditional attitude representations. A key innovation is the direct adaptive law that dynamically adjusts sliding manifold parameters, reducing reaching time and guiding the system toward desired dynamics once sliding is established. The controller is validated using the high-fidelity high-precision orbit propagator which accounts for the main environmental disturbances. Preliminary results demonstrate accurate attitude tracking performance in realistic maneuvering scenarios, confirming the controller's effectiveness for the challenging VLEO environment.

Introduction

The increasing interest in space missions operating in Very Low Earth Orbit (VLEO) has driven the development of advanced spacecraft attitude control strategies to ensure reliable performance in this challenging environment. In VLEO, perturbations arising from atmospheric drag become significant, requiring robust controllers to ensure precise pointing despite substantial uncertainties. In this context, a sliding mode–based attitude control law for VLEO spacecraft is proposed, designed to guarantee high pointing accuracy under severe disturbance and uncertainty conditions.

In this work, the attitude of the spacecraft is represented using rotation matrices defined on the Special Orthogonal Group $SO(3)$. This choice provides a unique, global, and nonsingular representation of orientation, avoiding the well-known issues of singularities, redundancy, and normalization constraints associated with Euler angles and quaternions.

Sliding Mode Control (SMC) is a widely used nonlinear control technique, recognized for its robustness to parametric uncertainties and external disturbances. SMC operates through a two-phase mechanism: first, system trajectories are driven in finite time toward a subset of the system states named sliding surface. Then, the trajectories evolve on this surface, yielding reduced-order dynamics with strong disturbance rejection properties.

Recent developments showed that a sliding surface can be defined directly on the Lie algebra associated with $\mathrm{SO}(3)$, thus preserving the intrinsic geometric structure of the attitude representation. This approach ensures global consistency and facilitates a systematic stability analysis [1,2].

Building upon these geometric formulations, this work introduces a time-varying SMC strategy that operates directly on $\mathrm{SO}(3)$. The proposed controller incorporates an adaptive mechanism that continuously adjusts the sliding manifold parameters in real time. During the reaching phase, this adaptation accelerates convergence by reshaping the manifold to align with the evolving system trajectories, while once sliding motion is achieved, the adaptive law steers the manifold toward the desired configuration, ensuring the intended closed-loop behavior [3].

Control framework on SO(3)

Attitude and velocity errors. Let $R(t) \in \mathrm{SO}(3)$ denote the current attitude of a rigid body and let $R_d(t) \in \mathrm{SO}(3)$ be a smooth, time-varying reference attitude. The corresponding body-fixed angular velocities are

$$\Omega = \left(R^\top \dot{R}\right)^\vee,\ \Omega_d = \left(R_d^\top \dot{R}_d\right)^\vee \in R^3, \tag{1}$$

where $(\cdot)^\vee : \mathfrak{so}(3) \to R^3$ is the vee operator and $\mathfrak{so}(3)$ is the Lie algebra of $\mathrm{SO}(3)$. The rotation error and angular velocity error are defined as

$$R_e = R_d^\top R \in \mathrm{SO}(3),\ \ \Omega_e = \Omega - R_e^\top \Omega_d \in R^3. \tag{2}$$

These errors quantify the geometric deviation of the current configuration from the desired trajectory directly on the manifold.

Kinematic Sliding Group and Control Law. Following the geometric sliding-mode design of [2,4], the sliding variable can be defined as follows:

$$s(R_e, \Omega_e) = \Omega_e + \lambda\, \Omega_u(R_e), \qquad \lambda > 0, \tag{3}$$

where log:$\mathrm{SO}(3) \to \mathfrak{so}(3)$ the matrix logarithm mapping the rotation error to the Lie algebra. Here, λ is a time-varying parameter according to the following adaptive law:

$$\dot{\lambda} = \mathrm{Proj}_{\lambda\in\Lambda}\left(-\gamma\, \mathrm{sign}(\langle J\Omega_u, s\rangle) - c\left(\lambda - \bar{\lambda}\right)\right), \tag{4}$$

where $\gamma >\ 0$ is an adaptation gain, and the Proj operator ensures λ remains in a feasible positive set $\Lambda \in R^+$. The adaptive law exhibits a two-term structure. The first term dominates when the system state is far from the sliding surface, accelerating convergence by dynamically steering the surface toward the system trajectories. As the sliding motion is established, this term vanishes, and the second term ensures that λ smoothly converges toward its desired nominal value $\bar{\lambda}$.

Finally, the control torque is designed as:

$$\tau_u = (J\Omega)^\wedge(\lambda\Omega_u(R_e) - \eta) - J\lambda\dot{\Omega}_u + J\dot{\eta} - Jk_s\langle Js, s\rangle^\sigma s + Jc\left(\lambda - \bar{\lambda}\right)\Omega_u(R_e), \tag{5}$$

where $k_s,\ \ > 0$ are control gains, $\bar{\lambda} > 0$ is final value reached by the λ parameter, η is the reference twist to be tracked expressed in the body frame, and $\langle\cdot,\cdot\rangle$ denotes the Euclidean inner product in R^3 and σ is a strictly positive value that varies between 0 and 0.5, in particular the latter

Materials Research Proceedings 69 (2026) 1083-1088 https://doi.org/10.21741/9781644904251-187

yields the discontinuous version of the controller. The resulting closed-loop system achieves almost-global stability on $SO(3)$, with finite-time reachability of the sliding manifold and exponential convergence in a neighborhood of the identity rotation matrix.

Simulation Environment

The spacecraft dynamics and control performance were evaluated using a high-fidelity six-degree-of-freedom numerical simulator developed in MATLAB/Simulink for VLEO operations. The simulator integrates coupled translational and rotational equations of motion in the Earth-Centered Inertial (ECI) reference frame, incorporating Earth's gravitational (EGM2008) and magnetic (IGRF-13) fields, atmospheric disturbances (NRLMSISE00), and solar radiation pressure (SRP). Attitude dynamics employ quaternion representation to avoid singularities, accounting for spacecraft inertia, environmental torques, control actuator torques, and momentum exchange with the reaction wheel (RW) assembly.

The simulation settings are reported in Table 1.

Table 1 Simulation settings including spacecraft properties, control hardware, sensor accuracy, initial conditions and space weather conditions.

	Parameter	Value
Spacecraft Mass Properties	Spacecraft Mass [kg]	29
	Inertia moments (I_{xx}, I_{yy}, I_{zz}) [kg/ m²]	1.117, 1.378, 0.508
	Residual Dipole (per axis) [Am²]	0.05
Control Hardware	RW Configuration	4-wheel pyramidal
	RW Tilt Angle [°]	26.57
	RW Saturation Momentum [Nms]	0.1
	RW Maximum Torque [mNm]	6
	Max. Magnetic Dipole [Am²]	2.6
Sensor Accuracy (1σ)	Position (X, Y) [mm]	1.5
	Position (Z) [mm]	1.25
	Velocity (X, Y) [mm/s]	0.015
	Velocity (Z) [mm/s]	0.03
	Angular Velocity [rad/s]	0.001
Initial Conditions	Epoch [UTC]	March 1, 2025, 10:00:00
	Position (ECI) [km]	[-2342.68, -6253.75, 0]
	Velocity (ECI) [km/s]	[-0.84, 0.32, 7.67]
	Euler Angles [°]	[0, 0, 0]
	Angular Velocity [°]	[0, 0, 0]
Space Weather Conditions (2001 Halloween storm)	$F_{10.7}$ (81-day-averaged, daily)	237
	Ap indeces	142

External disturbances encompass gravity gradient, magnetic, aerodynamic, and SRP torques. To minimize computational overhead, aerodynamic and SRP perturbations are pre-computed and stored in lookup tables rather than evaluated in real-time. The aerodynamic database, generated using the Cercignani–Lampis–Lord (CLL) gas–surface interaction model, combines data from a panel method in the free molecular flow regime [5] and high-fidelity Direct Simulation Monte Carlo (DSMC) runs in SPARTA [6] through a co-Kriging interpolation, increasing the accuracy of the aerodynamic force and torque coefficients parametrized by the angle of attack and sideslip angle relative to the body reference frame (BRF). The SRP database, computed via ray-tracing technique [7], contains force and torque distributions parametrized by solar azimuth and elevation angles with respect to the BRF. During propagation, disturbance forces and torques corresponding to instantaneous attitude configurations are retrieved through cubic spline interpolation of the lookup tables using the current relative orientation angles.

Materials Research Proceedings 69 (2026) 1083-1088 https://doi.org/10.21741/9781644904251-187

Results and Conclusions

The proposed control strategy enabled the spacecraft to successfully execute the complete multi-phase manoeuvre sequence, comprising slew, coast, and fine motion control phases, with smooth and stable dynamic behaviour.

Table 2 summarizes the time intervals associated with each manoeuvre phase, together with the selected convergence thresholds and the corresponding convergence times. The thresholds were chosen to both challenge the controller's performance and satisfy the mission requirements for fine pointing accuracy. The most stringent threshold corresponds to the onset of the fine motion phase, where the highest attitude precision is required.

The control frequency was set equal to the simulation integration step, i.e., 10 Hz, in accordance with the limitations of GNSS-based attitude measurements (here assumed to be available and aiding estimation) and the actuation bandwidth of the reaction wheels. Although higher control update rates are typically feasible, this frequency was assumed appropriate for the considered system constraints.

Despite the agility of the commanded profile, featuring pitch excursions of ±20° and angular rates on the order of 10^{-2} rad/s, the actuator torques remained unsaturated, Fig.2, exhibiting only brief peaks of less couple seconds during rapid slews. Across all phases, attitude convergence was achieved within a few seconds, as can be seen from Fig. 3, with steady-state errors consistently maintained below 0.01°.These results confirm the controller's effectiveness in achieving precise attitude tracking under the simulated dynamic and demanding VLEO conditions.

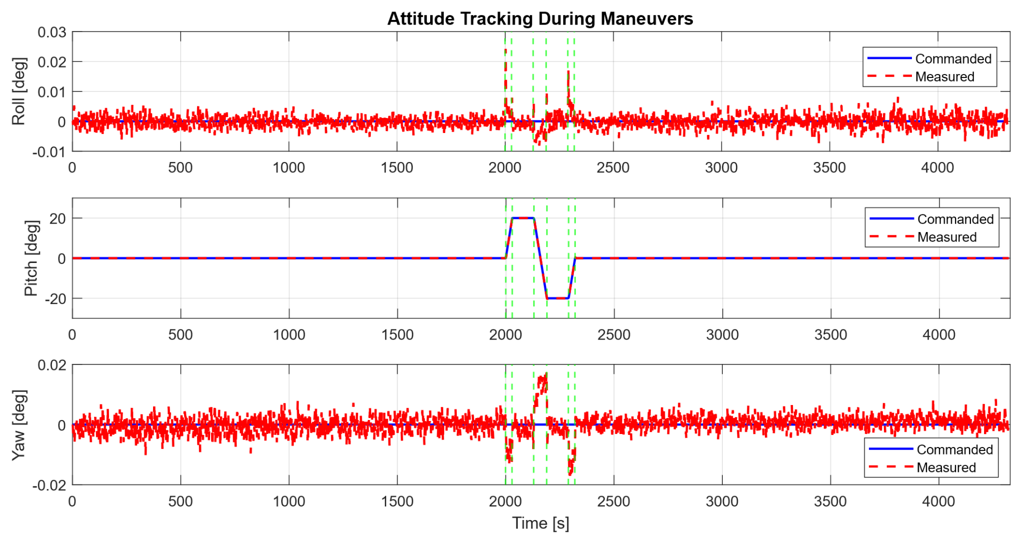

Figure 1. Commanded and measured Euler angles during the manoeuvre

Table 2. Time intervals of the different manoeuvre phases and respective convergence times and tolerances thresholds.

	Time interval [s]	Error threshold [°]	Convergence time [s]
Case 1	1998-2029	0.5	2.5
Case 2	2029-2129	0.5	2.1
Case 3	2129-2189	0.2	3.2
Case 4	2189-2289	0.5	2.2
Case 5	2289-2319	0.5	2.5
Case 6	2319-3000	0.5	2

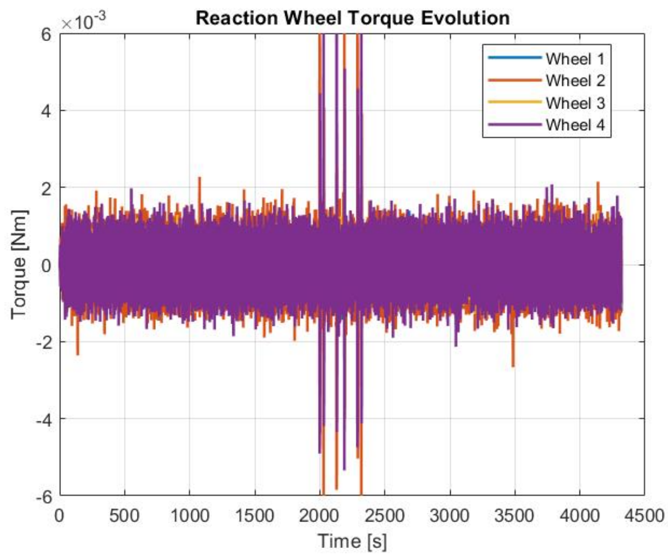

Figure 2. Distributed actuated torque on the RWs pyramidal configuration.

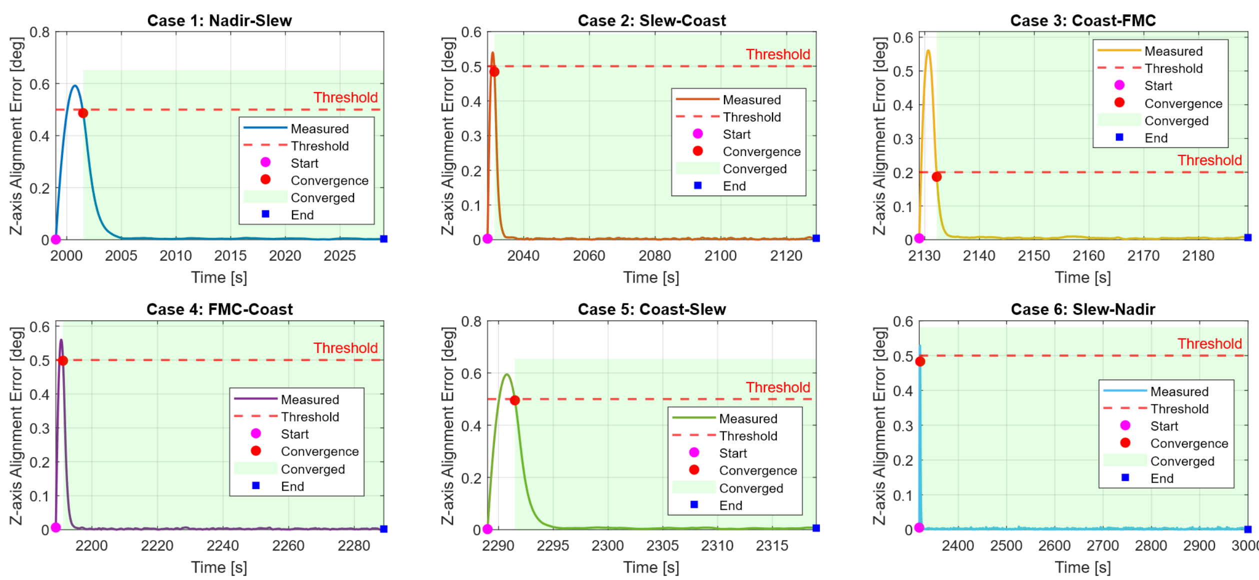

Figure 3. Convergence analysis for the separate phases of the manoeuvre.

Acknowledgements

This work was carried out within the *Space It Up!* project funded by the Italian Space Agency (ASI) and the Italian Ministry of University and Research (MUR) under contract No. 2024-5-E.0, CUP No. I53D24000060005.

References

[1] Francesco Bullo and Andrew D Lewis. Geometric Control of Mechanical Systems. Vol. 49. Texts in Applied Mathematics. Springer, 2004.

[2] Eduardo Espindola and Yu Tang. “Geometric sliding mode control of mechanical systems on Lie groups”. In: Automatica 177 (2025), p. 112346. issn: 0005-1098. doi:

https : / / doi . org / 10 . 1016 / j . automatica . 2025 . 112346

[3] M.Mancini. “Adaptive Variable Structure Control System for Attitude Spacecraft Applications”. PhD thesis. Politecnico di Torino, 2023.

[4] Qingkai Meng, Hao Yang, and Bin Jiang. “Second-order sliding-mode on SO(3) and fault-tolerant spacecraft attitude control”. In: Automatica 149 (2023), p. 110814. issn: 0005-1098. doi: https : / / doi . org / 10 . 1016 / j . automatica . 2022 . 110814.

[5] Sinpetru, L. A., Crisp, N. H., Mostaza-Prieto, D., Livadiotti, S., and Roberts, P. C. E., “ADBSat: Methodology of a Novel Panel Method Tool for Aerodynamic Analysis of Satellites,” *Computer Physics Communications*, Vol. 278, 2022, p. 108456. https://doi.org/10.1016/j.cpc.2022.108456

[6] Plimpton, S. J., Moore, S. G., Borner, A., Stagg, A. K., Koehler, T. P., Torczynski, J. R., and Gallis, M. A., “Direct Simulation Monte Carlo on Petaflop Supercomputers and Beyond,” *Physics of Fluids*, Vol. 31, No. 8, 2019. https://doi.org/10.1063/1.5108534

[7] Li, Z., Ziebart, M., Bhattarai, S., Harrison, D., and Grey, S., “Fast Solar Radiation Pressure Modelling with Ray Tracing and Multiple Reflections,” *Advances in Space Research*, Vol. 61, No. 9, 2018, pp. 2352–2365. https://doi.org/10.1016/j.asr.2018.02.019